

A Mechanistic Understanding of Stress Corrosion Cracking of Mg-Al Alloys

N. Winzer^{1,a}, A. Atrens^{2,b}, W. Dietzel^{3,c}, V.S. Raja⁴, G. Song², K.U. Kainer³

¹ Division V.5, Bundesanstalt für Materialforschung und -prüfung, Berlin, 12205, Germany

² Materials Engineering, The University of Queensland, Brisbane 4072, Australia

³ Institute for Materials Research, GKSS-Forschungszentrum Geesthacht GmbH, D-21502, Geesthacht, Germany

⁴ Department of Metallurgical and Materials Science, Indian Institute of Technology, Powal, Mumbai 400 076, India

^a nickwinz@graduate.uwa.edu.au, ^b andrejs.atrens@uq.edu.au, ^c wolfgang.dietzel@gkss.de

Keywords: stress corrosion cracking, hydrogen embrittlement, magnesium alloys, constant extension rate test (CERT)

Abstract. The influence of alloying and microstructure on the mechanism(s) for Stress Corrosion Cracking (SCC) of Mg-Al alloys in distilled water has been investigated by Constant Extension Rate Tests (CERTs) of the alloys AZ91 (which consists of an α -matrix with extensive β -particles), AZ31 (which consist of an α -matrix with similar Al concentration to that in AZ91) and AM30 (which has a composition similar to AZ31 but with lower concentrations of Zn and second phase particles). For AZ31 and AM30, SCC initiation and propagation occur by localised dissolution and Hydrogen Embrittlement (HE) respectively. There is a difference in the mechanism or critical (rate limiting) process for HE in AZ31 and AM30, which may be related to the influences of Zn and second phase particles on the diffusivity of H in the α -matrix. The mechanism for SCC initiation in AZ91 is uncertain; however, it does not occur by localised dissolution as per AZ31 and AM30. SCC propagation in AZ91 at moderate strain rates involves crack nucleation within β -particles ahead of the principal crack tip, and HE of the α -matrix by a mechanism similar to that in AZ31. AZ91 specimens tested in air after charging in H₂ gas to induce hydride precipitation had a similar fracture surface morphology to specimens tested in distilled water at very slow strain rates, suggesting a mechanism involving MgH₂ precipitation.

Introduction

Recent publications [1, 2, 3, 4, 5, 6, 7, 8] have shown that there exists a considerable body of research outlining the phenomenology of Transgranular Stress Corrosion Cracking (TGSCC) of Mg alloys. It is generally accepted that the mechanism for TGSCC of Mg alloys is Hydrogen Embrittlement (HE) with the hydrogen coming from the cathodic partial reaction (hydrogen generation) of the Mg corrosion reaction [9, 10, 11, 12]; however, the specific nature of the HE mechanism remains uncertain. The HE models that may be applicable for Mg alloys are: Hydrogen Enhanced Decohesion (HEDE); Hydrogen Enhanced Localised Plasticity (HELP); Adsorption Induced Dislocation Emission (AIDE); and Delayed Hydride Cracking (DHC). AIDE [13] and DHC [14, 15, 16, 17] have been proposed for TGSCC of Mg alloys; however, the evidence for both mechanisms is limited. HEDE and HELP also remain possibilities. An understanding of the influences of microstructure, environment and mechanical loading on the potential mechanisms for SCC of Mg alloys is in high demand due to the rapidly growing interest in Mg alloys for stressed automobile components. The work presented herein summarizes the results of the initial phase of an ongoing research program, which is ultimately aimed at developing a methodology for minimising

susceptibility by microstructural modification. This paper identifies key issues to be addressed in developing a mechanistic understanding of SCC of Mg alloys.

Experimental Method

The test materials were the Mg alloys AZ91, AZ31 and AM30, which contained 8.9%Al–0.8%Zn–0.2%Mn, 2.6%Al–0.8%Zn–0.6%Mn and 2.9%Al–0.4%Mn respectively. AZ91 specimens were machined from as-cast ingots, whereas AZ31 and AM30 specimens were machined from large extrusions such that their tensile axis was parallel with the extrusion direction. The grain sizes were 50 – 100 μm for AZ91 and 1 – 2 μm for AZ31 and AM30 (equiaxed in all cases). All alloys were machined into cylindrical tensile specimens with a 5 mm diameter waisted gauge section. AZ91 contained an extensive interdentritic β -phase ($\text{Mg}_{17}\text{Al}_{12}$ [9, 10, 17, 18, 19, 20]), fine plate-like crystals within the interdendritic phase (30%Mg, 47%Al, 23%Mn) and small intragranular precipitates (45%Al, 55%Mn). AZ31 and AM30 contained a sparse dispersion of $\sim 10 \mu\text{m}$ quadrilateral plate-like crystals (21wt%Al, 79wt%Mn), $\sim 3 - 4 \mu\text{m}$ interdendritic particles ($>20\text{wt}\%\text{Si}$), and elongated $\sim 3-6 \mu\text{m}$ plate-like crystals that were aligned collinearly in the extrusion direction ($>30\%\text{Al}$, $>40\%\text{Mn}$). The quadrilateral plate-like crystals were larger and more numerous for AZ31 than for AM30. The test environment was double-distilled H_2O at room temperature and open circuit conditions. Control tests were carried out in laboratory air. The mechanical load on the specimen was applied under Constant Extension Rate Test (CERT) conditions. The apparent strain rates are given in Table 1. The threshold stress for SCC, σ_{SCC} , was measured using the DC Potential Drop (DCPD) method. σ_{SCC} was interpreted as the stress corresponding to the deviation of the DCPD curve from initial linearity. The stress corrosion crack velocity, V_c , was calculated from $\Delta a/\Delta t_{\text{SCC}}$, where Δa is the maximum size of the SCC fracture surface zone and Δt_{SCC} is the time between crack initiation (furnished by the DCPD measurements) and the end of the test.

		AZ91 ($\sigma_Y=70\text{MPa}$, UTS=165MPa)				AZ31 ($\sigma_Y=180\text{MPa}$, UTS=250MPa)					AM30 ($\sigma_Y=175\text{MPa}$, UTS=230 MPa)		
$\delta\varepsilon/\delta t$	$\times 10^{-8} \text{ s}^{-1}$	3	10	30	50	5	10	20	50	80	10	30	50
$\sigma_{\text{SCC}}/\sigma_Y$	MPa	0.79	0.86	1.1	1.0	0.58	0.81	0.92	0.89	0.94	0.80	0.74	0.80
V_c	$\times 10^{-9} \text{ m/s}$	1.6	3.7	10.5	12.0	4.4	2.0	6.7	1.2	5.5	0.36	0.93	0.55

Table 1 - SCC parameters for AZ91, AZ31 and AM30 at various strain rates.

Results

SCC Characteristics. Figs. 1-3 show the stress versus apparent strain curves for AZ91, AZ31 and AM30, in distilled water and laboratory air, under CERT conditions. For specimens in distilled water, the apparent plastic deformation is largely attributed to SCC, with some contribution by the inert fracture mode, particularly at higher strain rates. In laboratory air, AZ91 had a lower σ_Y , higher strain hardening rate and lower ductility relative to AZ31 and AM30. The lower σ_Y is attributed to the larger grain size for AZ91. The lower ductility of AZ91 is largely attributed to the presence of β -particles [21, 22]. The higher strain hardening rate may be attributable to both the larger grain size and the presence of β -particles. In distilled water, all alloys suffered a reduction in UTS and apparent ductility relative to tests in laboratory air, with the UTS and apparent ductility decreasing with decreasing strain rate. The apparent ductility of AZ31 was considerably more sensitive to changes in strain rate than that of AZ91 and AM30. The SCC parameters, $\sigma_{\text{SCC}}/\sigma_Y$ and V_c , for each strain rate ($\delta\varepsilon/\delta t$) are summarised in Table 1. $\sigma_{\text{SCC}}/\sigma_Y$ tended towards 0.6 for AZ91 and AZ31 and was ~ 0.75 for AM30. There was a decrease in σ_{SCC} with decreasing strain rate for AZ91 and AZ31 (see also Fig. 2 for AZ31); however, this trend was not identified for AM30 due to the narrower range of strain rates. There was an increase in V_c with increasing strain rate for AZ91. In contrast,

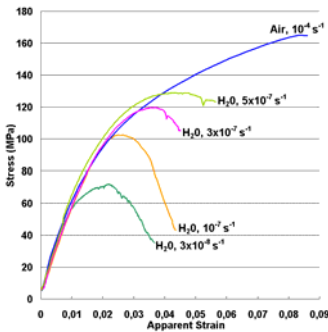


Fig. 1 - Stress vs apparent strain curves for AZ91.

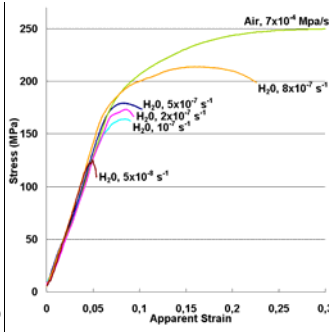


Fig. 2 - Stress vs apparent strain curves for AZ31.

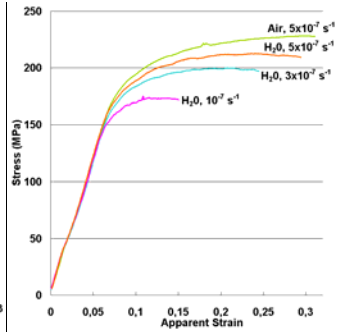


Fig. 3 - Stress vs apparent strain curves for AM30.

V_c appeared independent of strain rate for AZ31 and AM30. V_c was considerably lower for AM30 than for AZ91 and AZ31, whilst V_c for AZ31 was slightly lower than for AZ91.

Secondary Cracking. Secondary cracks were apparent on the gauge surfaces of AZ91, AZ31 and AM30 specimens fractured in distilled water. The density of secondary cracks in AZ91 specimens was considerably lower than in AZ31 and AM30 specimens. In all cases the secondary cracks were normal to the loading direction. Secondary cracks in AZ91 specimens were macroscopically sharp, with cracks nucleating within β -particles ahead of the principle crack tip and propagating transgranularly in a relatively constant direction (Fig. 4). Cracks within β -particles were generally normal to the loading direction, indicating that β -particles fracture in favour of the surrounding matrix in response to mechanical loading. Perpendicular cliffs were formed between converging

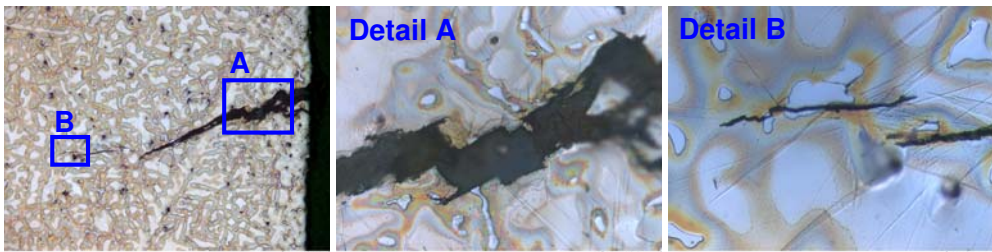


Fig. 4 – Secondary crack in AZ91 specimen.

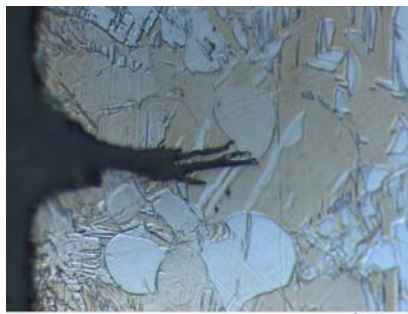


Fig. 5 – Secondary crack in AZ31 specimen (similar secondary cracks occurred in AM30).

consecutive cracks, which undercut the cliffs by $\sim 10 \mu\text{m}$. Secondary cracks in AZ31 and AM30 specimens were typically $100 - 200 \mu\text{m}$ deep and often diverged into several roughly-parallel tunnels (Fig. 5). They appeared to be due to highly localised dissolution; however, the dissolution did not occur adjacent to second phase particles, as is typical for two-phase Mg-Al alloys in aggressive environments [9, 10]. Such crack initiation by highly localised dissolution did not occur for testing under Linearly Increasing Stress Test (LIST) conditions [3] indicating that the crack initiation by highly localised dissolution is a peculiarity of CERT testing.

SCC Fracture Surface Morphology. The SCC fracture surfaces for AZ91 specimens tested at $10^{-7} - 5 \times 10^{-7} \text{ s}^{-1}$ in distilled water contained multiple thumbnail-shaped SCC zones, which were characterised by: (i) parallel facets $\sim 5 \mu\text{m}$ wide; (ii) jogging at the edges of each facet; (iii) extensive crack branching; and (iv) cleavage through β -particles (Fig. 6). The faceted appearance of the fracture surface may be related to the formation of perpendicular cliffs between consecutive secondary cracks (Fig. 4b). Examination at high magnification revealed that the parallel facets contained fine parallel markings ($< 0.5 \mu\text{m}$ apart) or ellipsoidal micro-dimples. The orientation of the parallel facets and fine parallel markings was influenced by β -particles (Figs. 6-7). For specimens tested at $10^{-7} - 5 \times 10^{-7} \text{ s}^{-1}$, the non-SCC fracture surface regions were comprised of broken, jagged features consistent with fracture in laboratory air. In contrast, for specimens tested at $3 \times 10^{-8} \text{ s}^{-1}$, the non-SCC fracture surface regions were comprised of smooth, rounded features somewhat comparable to shrinkage porosity [23], interspersed with small ($< 50 \mu\text{m}$ across) regions of broken, jagged facets consistent with fracture in laboratory air (Fig. 8). These “quasi-porous” features were similar to those found on fracture surfaces for AZ91 specimens pre-charged in H_2 gas at $300 \text{ }^\circ\text{C}$ and 30 bar for 15 h, and attributed to precipitation, fracture and decomposition of metastable MgH_2 particles [5].

The SCC fracture surfaces for AZ31 and AM30 specimens consisted of three separate morphologies: (i) a 100 to $200 \mu\text{m}$ wide region at the gauge surface consistent with severe localised dissolution; (ii) a macroscopically-flat SCC “band”; and (iii) a final overload fracture region consistent with fracture in an inert environment (Fig. 9). The width and morphology of the localised dissolution regions corresponded with the depth and morphology of secondary cracks in AZ31 and AM30 specimens tested in distilled water under CERT conditions, as shown in Fig. 5. The SCC band for AZ31 was characterised by quasi-crystallographic markings containing small ($< 0.5 \mu\text{m}$ across) specifically oriented ellipsoidal dimples (Fig. 10). The dimples were similar to those observed within parallel facets on SCC fracture surfaces for AZ91 (Fig. 6). In contrast with that for AZ31, the SCC band for AM30 was characterised by distinctly cleavage-like markings, with coarse, pit-like features and tunnels (attributed to filigree corrosion on the crack surface) that diminished in size and density with increasing distance from the gauge surface (Fig. 11).

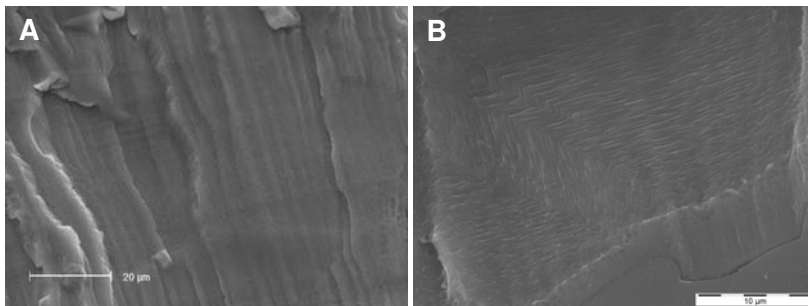


Fig. 6 – SCC fracture surface for AZ91 showing (A) parallel facets and (B) fine parallel markings.

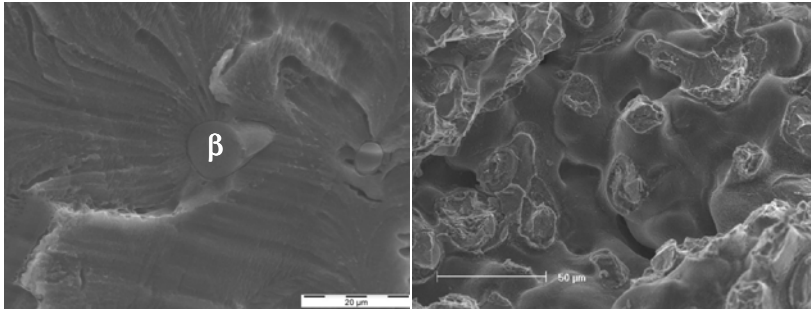


Fig. 7 – SCC fracture surface for AZ91 showing the influence of β -particles on the orientation of parallel markings.

Fig. 8 – Fracture surface morphology for AZ91 in distilled water at $3 \times 10^{-8} \text{ s}^{-1}$ showing quasi-porous features.

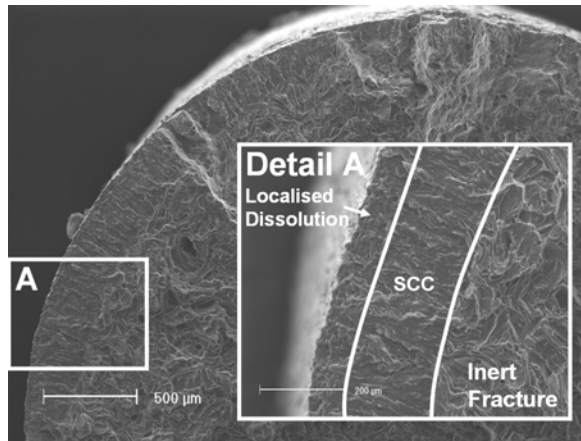


Fig. 9 – Fracture surface for AM30 in distilled water under CERT conditions showing zones corresponding to localised dissolution, SCC and inert fracture. Fracture surfaces for AZ31 in distilled water were similarly composed.

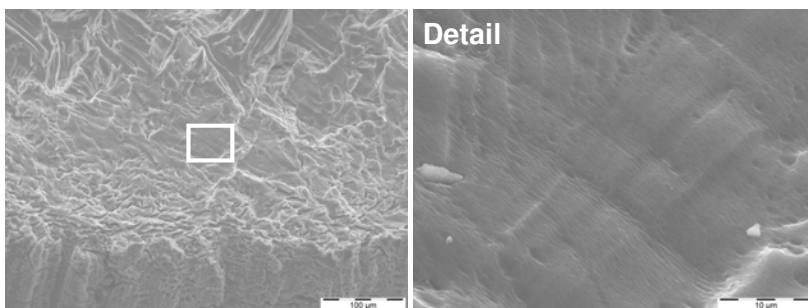


Fig. 10 – Morphology of SCC band for AZ31.

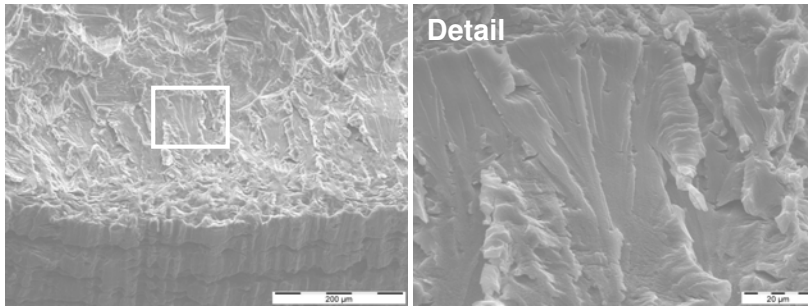


Fig. 11 – Morphology of SCC band for AM30.

Discussion

Fig. 5 shows that, for AZ31 and AM30 specimens, SCC initiation occurred by localised dissolution. It is uncertain why localised dissolution occurs independently of any microstructural features, although one possibility is that it occurs at sites of mechanical film rupture caused by emerging slip steps. Fig. 10 shows that a transition in the mechanism for SCC of AZ31 and AM30 occurs when the crack length is 100 – 200 μm . The fractography corresponding to propagation beyond this critical crack length is indicative of a mechanism involving HE. Some difference in the mechanism or critical (rate limiting) process for HE in AZ31 and AM30 is indicated by: (i) the lower V_c for AM30 relative to AZ31 (see Table 1); (ii) the contrast in the fracture surface morphologies for AZ31 (Fig. 10) and AM30 (Fig. 11). These differences may be related to the influences of Zn and second phase particles (which were more concentrated in AZ31) on the diffusivity of H in the α -matrix. The difference in H diffusivity for AZ31 and AM30 could be such that: (i) different HE mechanisms occur in each alloy; or (ii) that the same HE mechanism occurs, with the difference in H diffusivity affecting V_c and the fracture surface morphology (the crystallographic orientation of the cleavage-like facets and the size of the micro-dimples).

Fig. 4 shows that SCC initiation in AZ91 does not occur by localised dissolution as per AZ31 and AM30. The SCC fracture surface morphology for AZ91 is indicative of a mechanism involving HE. It is clear that β -particles play an important role in this mechanism, as evidenced by: (i) the nucleation of stress corrosion cracks within β -particles ahead of the principal crack tip; (ii) the influence of β -particles on the orientation of fine parallel markings and ellipsoidal micro-dimples on the fracture surface; and (iii) the lower σ_{SCC} for AZ91 relative to AZ31. The nucleation of stress corrosion cracks within β -particles ahead of the principal crack tip may be due to: (i) the inherently low fracture toughness of the β -particles; or (ii) a reduction in the fracture toughness of β -particles by internal hydrogen. Recently, Chen et al [24] showed that immersion of AZ91 in Na_2SO_4 solution (cathodically polarised and at the free corrosion potential) in the absence of external stress resulted in fracture of β -particles at the surface, indicating that the fracture of β -particles is indeed due to H and not their inherently low fracture toughness. Thus, the increase in SCC susceptibility of Mg-Al alloys with increasing Al concentration [18] may be related to the propensity for crack nucleation within β -particles. Moreover, if the mechanism for SCC propagation involves H transport with mobile dislocations (as per HELP), then the influence of strain rate may be mitigated by the presence of H at multiple internal sources [25]. Thus, if β -particles behave as reversible H traps (i.e. as sinks and sources), this may explain why the elongation-to-failure for AZ31 (which consists of an α -matrix only) is more dependent on strain rate than that for AZ91 (which contains β -particles). An alternative explanation for the higher strain rate sensitivity of AZ31 is related, as per the discussion in Winzer et al [4], to: (i) the higher SCC initiation stress; and (ii) a SCC velocity independent of applied strain rate.

It was previously proposed that MgH_2 particles may be precipitated in AZ91 by pre-charging in H_2 gas at 300 °C and 30 bar for 15 h [5]. This was corroborated by numerical analysis of the H concentration imparted by pre-charging, and the reduction in the H solvus concentration upon cooling to room temperature (although it should be noted that this analysis used speculative values for the solvus concentration). The fracture surfaces for AZ91 specimens tested in laboratory air after pre-charging in H_2 gas [5] were similar to those for specimens tested in distilled water at $3 \times 10^{-8} \text{ s}^{-1}$. This implies that for SCC of AZ91 at crack velocities $< 1.6 \times 10^{-9} \text{ m/s}$, the quantity of H transported ahead of the crack tip is sufficient for precipitation of MgH_2 particles.

The specific mechanism(s) for SCC propagation in AZ91, AZ31 and AM30 remain uncertain. The occurrence of micro-dimples on AZ91 and AZ31 SCC fracture surfaces is consistent with a mechanism involving microvoid nucleation (HELP and/or AIDE). In the case of AZ31, the micro-dimples occurred within macroscopically flat, quasi-crystallographic facets. Observations of dimples within cleavage-like facets on SCC fracture surfaces have been ascribed to AIDE by other workers [13, 26]; however, in the present case it has not been determined whether the dimpled facets correspond to a specific crystallographic plane. In contrast, cleavage-like fracture surfaces, such as those observed in the present work for AM30 (see Fig. 11), are typically associated with HEDE [27, 28]; however, it is also possible that micro-dimples do occur on the SCC fracture surfaces for AM30, albeit on a smaller scale than for AZ31.

Conclusions

- The mechanism for SCC initiation in AZ31 and AM30 involves transgranular localised dissolution, possibly due to mechanical film rupture at emerging slip steps.
- For AZ31 and AM30, the mechanism for crack growth changes from localised dissolution to HE at some critical crack length. There were differences in the mechanisms or critical (rate limiting) processes for HE in AZ31 and AM30, manifested in: (i) V_c ; (ii) the crystallography of cleavage-like fracture surface markings; and (iii) the appearance of micro-dimples within the cleavage-like facets. These differences were attributed to the influences of Zn and second phase particles (concentrated in AZ31) on H diffusivity in the α -matrix. The influences of Zn and second phase particles could be such that: (i) different HE mechanisms occur for AZ31 and AM30; or (ii) the same HE mechanism occurs in AZ31 and AM30, with the difference in H diffusivity affecting V_c and the fracture surface morphology.
- The mechanism for SCC initiation in AZ91 is uncertain; however, it does not occur by localised dissolution as per AZ31 and AM30.
- β -particles play an important role in SCC of AZ91, as evidenced primarily by the nucleation of stress corrosion cracks within β -particles ahead of the principal crack tip. Crack nucleation within β -particles is probably due to a reduction in their fracture toughness by trapped hydrogen. The role of β -particles implies that the increasing SCC susceptibility of Mg alloys with increasing Al concentration is related to the distribution of, and propensity for crack nucleation within, β -particles.
- The fracture surfaces for AZ91 specimens tested in distilled water at very slow strain rates were similar to those resulting from pre-charging in gaseous H_2 to induce hydride precipitation, implying that the quantity of H transported ahead of the crack tip during SCC of AZ91 at very slow crack velocities is sufficient for hydride precipitation.

References

- [1] N. Winzer, A. Atrens, G. Song, E. Ghali, W. Dietzel, K.U. Kainer, N. Hort and C. Blawert: Adv. Eng. Mater. Vo. 8 (2005), p. 659

- [2] N. Winzer, A. Atrens, W. Dietzel, G. Song and K.U. Kainer: *Mat. Sci. Eng. A* Vol. 466 (2007), p. 18
- [3] N. Winzer, A. Atrens, W. Dietzel, G. Song and K.U. Kainer: *Mat. Sci. Eng. A* Vol. 472 (2008) p. 97
- [4] N. Winzer, A. Atrens, W. Dietzel, V.S. Raja, G. Song and K.U. Kainer: *Mat. Sci. Eng. A* doi:10.1016/j.msea.2007.11.064 (2008)
- [5] N. Winzer, A. Atrens, W. Dietzel, G. Song and K.U. Kainer: *Metall. Mater. Trans.* Vol. 39 (2008), p. 1157
- [6] N. Winzer, A. Atrens, W. Dietzel, G. Song and K.U. Kainer: *Adv. Eng. Mater.* doi:10.1002/adem.200700319 (2008)
- [7] M. Bobby Kannan, W. Dietzel, C. Blawert, A. Atrens and P. Lyon: *Mat. Sci. Eng. A* Vol. 480 (2007), p. 529
- [8] R.G. Song, C. Blawert, W. Dietzel and A. Atrens: *Mater. Sci. Eng.* Vol. 399 (2005), p. 308
- [9] G. Song and A. Atrens: *Adv. Eng. Mater.* Vol. 1 (1999), p. 11
- [10] G. Song and A. Atrens: *Adv. Eng. Mater.* Vol. 5 (2003), p. 837
- [11] G. Song and A. Atrens: *Adv. Eng. Mater.* Vol. 9 (2007), p. 177
- [12] A. Atrens and W. Dietzel: *Adv. Eng. Mater.* Vol. 9 (2007), p. 292
- [13] S.P. Lynch and P. Trevena: *Corrosion* Vol. 44 (1988), p. 113
- [14] E.I. Meletis and R.F. Hochman: *Corrosion* Vol. 40 (1984), p. 39
- [15] D.G. Chakrapani and E.N. Pugh: *Metall. Trans. A* Vol. 7A (1976), p. 173
- [16] A.J. Bursle and E.N. Pugh, in: *Mechanisms of Environment Sensitive Cracking of Materials*, edited by P.R. Swann, F.P. Ford and A.R.C. Westwood, Materials Society, London (1977), p. 471
- [17] G.L. Makar, J. Kruger and K. Sieradzki: *Corros. Sci.* Vol. 34 (1993), p. 1311
- [18] L. Fairman and H.J. Bray: *Corros. Sci.* Vol. 11 (1971), p. 533
- [19] W.M. Pardue, F.H. Beck, M.G. Fontana: *Trans. Am. Soc. Met.* Vol. 54 (1961), p. 539
- [20] W.K. Miller, in: *Stress Corrosion Cracking: Materials Performance and Evaluation*, edited by R.H. Jones, ASM International, USA (1992), p. 251
- [21] W.F. Hosford and R.M. Cadell, *Metal Forming Mechanics and Metallurgy 2nd Ed* (Prentice-Hall, NJ 1993)
- [22] M.C. Zhao, M. Liu, G. Song, A. Atrens: *Adv. Eng. Mater.* Vol. 10 (2008), p. 93.
- [23] A. Munitz, C. Cotler, A. Stern, G. Kohn: *Mat. Sci. Eng. A* Vol. 302 (2001), p. 68
- [24] J. Chen, J. Wang, E. Han, J. Dong, W. Kei: *Corros. Sci.* Vol. 50 (2008), p. 1292
- [25] G.M. Pressouyre: *Acta Metall.* Vol. 28 (1980), p. 895
- [26] S.P. Lynch: *Acta Metall.* Vol. 34 (1988), p. 2639
- [27] H.K. Birnbaum, in: *Hydrogen Effects on Material Behavior*, edited by N.R. Moody and A.W. Thompson, TMS, Warrendale (1990), p. 639
- [28] R.P. Gangloff, in: *Comprehensive Structural Integrity*, edited by I. Milne, R.O. Ritchie and B. Karihaloo, Vol. 6.02, Elsevier, Oxford (2003), p. 31